Open Access

Nano-Scale Lateral Milling with Focused Ion Beam for Ultra-Smooth Optical Device Surface

Yeonjoon Park[*,1], SangJoon Park[2], Uhn Lee[3] and Sang H. Choi[4]

[1]*National Institute of Aerospace, Hampton, VA 23666, USA*

[2]*Chemistry Department, Kyungwon University, Kyungki-do, 461-701, Korea*

[3]*Gacheon University of Medicine and Science, Incheon, 405-760, Korea*

[4]*NASA Langley Research Center, Hampton, VA 23681, USA*

Abstract: The effect of the nano-scale lateral milling process using a focused ion beam (FIB) was studied in order to prepare a flat and smooth surface suitable for the growth of optical device structures such as a distributed Bragg reflector (DBR) mirror on a rough gallium nitride (GaN) surface. A high-quality, smooth, and flat surface is very essential for high precision space optics. It was fabricated using the nano-scale lateral milling process and was analyzed using an atomic force microscope. A regular geometric corrugation ripple with an amplitude of 18Å was achieved using a 30 KeV gallium ion-beam oriented at a normal angle of incidence operating at a beam current of 7nA. We suggest a simple engineering model for the formation of regular geometric ripples made by the serial cutting sequence of focused ion beam. This model can improve various device fabrications with a focused ion beam.

Keywords: Lateral milling, FIB, ring grating, nano milling, ultra smooth milling, micro spectrometer.

1. INTRODUCTION

Currently, a group of scientists at NASA Langley Research Center are developing a patent-pending micro-spectrometer for space exploration which is based on the Fresnel diffraction method [1-3]. The core function of micro-spectrometer is performed for differentiating and forming various color cones along the optical axis by a micro-zone plate. A spectral resolution of 23nm was achieved with an ultra small micro zone plate of 750μm diameter and 532nm wavelength [3]. Micro-zone plate as a key element of micro-spectrometer requires an extremely fine machining for high quality of smoothness and flatness to meet the optical resolution (see Fig. **1**). Micro-spectrometer optical systems for NASA's space applications, as shown in Fig. (**2**), require very high resolutions ($< \lambda/30$) and stability that may be possible by only nanoscale precision machining using a focused ion beam (FIB) system.

A focused ion beam is an ideal fabrication tool for rapid prototyping of micro and nano structures [2]. A highly accelerated gallium ion beam bombards and removes target materials in a narrow focal point to fabricate desired shapes. Enhanced etching and material deposition are achieved using special processing gas injections into the processing region. Surface milling and etching by a FIB system enhances the optical characteristics of micro-optical devices by reducing the roughness of optical surfaces and improves the exactness of optical edges by utilizing the FIB's precision nanoscale machining capability. Such an enhancement is essential for the rapid fabrication of micro-optical devices with high optical performance, such as diode lasers and micro-spectrometers [3]. This also facilitates the development of smart optical materials by providing the accurate optical boundaries and optical fields necessary to interrogate the performance of the material.

While a typical focused ion beam milling is performed vertically at a glancing angle on the sidewall of an object such as a Transmission Electron Microscope (TEM) sample for Omni-probe transfer, the lateral milling of materials with a focused ion beam where ion beam comes from the normal angle perpendicular to the surface is also important to obtain an optically-flat surface to avoid the distortion and scattering of transmitted and reflected light. For example, Fig. (**1a**) shows a differential interference contrast microscope image of a ~750 μm Fresnel zone plate made using a gallium focused ion beam without any process gasses injected during the milling process. Fig. (**1b**, **c**) are Scanning Electron Microscope (SEM) images showing the presence of residual materials and a rough surface on the Fresnel zone plate. Unclean gaps between the Fresnel rings are observed, which will lead to a reduced performance of the Fresnel zone plate. The materials in unclean gap came from re-deposition of materials during long time of sequential cuttings and incomplete material removal process at the Gallium ion beam etched area. Fig. (**1d**) also shows a side-effect of circular cutting with focused ion beam as small concentric ripples are unintentionally generated on each ring. Such imperfections of FIB processed materials can cause a decrease in light intensity, distortion of the optical wavefront, and a loss of coherence for the optical device. Therefore, it is important to study the effect of the focused ion beam milling processes on the surface corrugation. In addition, in order to make patterning on the surface, the ion

*Address correspondence to this author at the National Institute of Aerospace, Hampton, VA 23666, USA; Tel: 757-864-9196;
E-mail: y.park@nianet.org

1877-6116/10 2010 Bentham Open

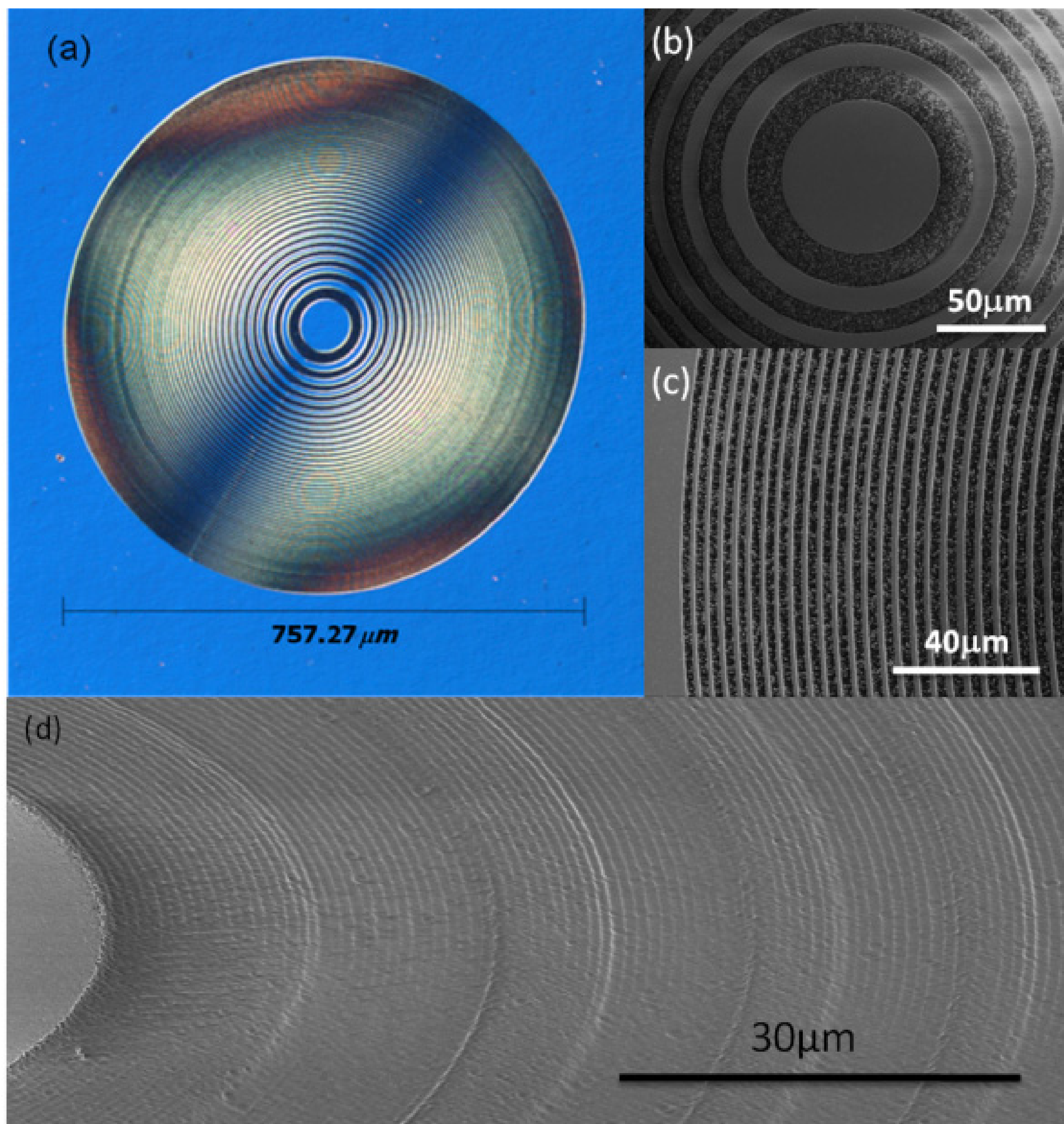

Fig. (1). (**a**) Optical microscope image of a Fresnel zone plate made by a focused ion beam (FIB) milling process. SEM images of (**b**) the center region and (**c**) the edge region of the zone plate showing residual gallium droplets and the appearance of a rough surface. (**d**) SEM image of another circular grating shows small concentric ripples that are unintentionally made by circular cutting with the FIB.

beam has to enter from a perpendicular direction to the surface to transfer a pattern isotropically. Therefore, our paper describes the FIB milling effect from a perpendicular direction on the surface to make patterns like small optical device structures. However, any pattern is made of sum of small flat area. Thus, in order to study FIB milling effect in detail, it is best to create a large flat area without walls and study the residual flatness.

We studied residual surface corrugation effect of FIB surface milling with GaN materials because GaN is one of the most important wide bandgap semiconductors which are used in blue and UV light emitting diodes (LEDs) and edge emitting laser diodes [4-6]. Recently, the fabrication of vertical cavity surface emitting laser (VCSEL) diodes using GaN materials has been reported [7-9]. However, several difficulties still hinder the fabrication of high-quality GaN VCSEL diodes [10,11]. It is difficult to build a high quality (high-Q) optical resonator because of the inherent difficulties of performing epitaxial growth on a polarized surface [12]. Also, because there is a large lattice mismatch of AlGaN on GaN, it is very difficult to grow morphological AlGaN with more than a 25% Al content on GaN [11]. In addition, the small refractive index difference between AlGaN and GaN requires more than 70 DBR layers fabricated with strict precision to achieve a high reflectivity (>99.9%). In comparison, an AlAs/GaAs DBR used for an IR-VCSEL requires only 20 layers to achieve 99.9% reflectivity. Finally, the low electrical conductivity of the AlGaN/GaN DBR and the p-GaN layers results in a low current injection efficiency through the top layer [13].

To improve the quality of DBR mirrors, the flatness of the GaN surface has to be improved before the epitaxial

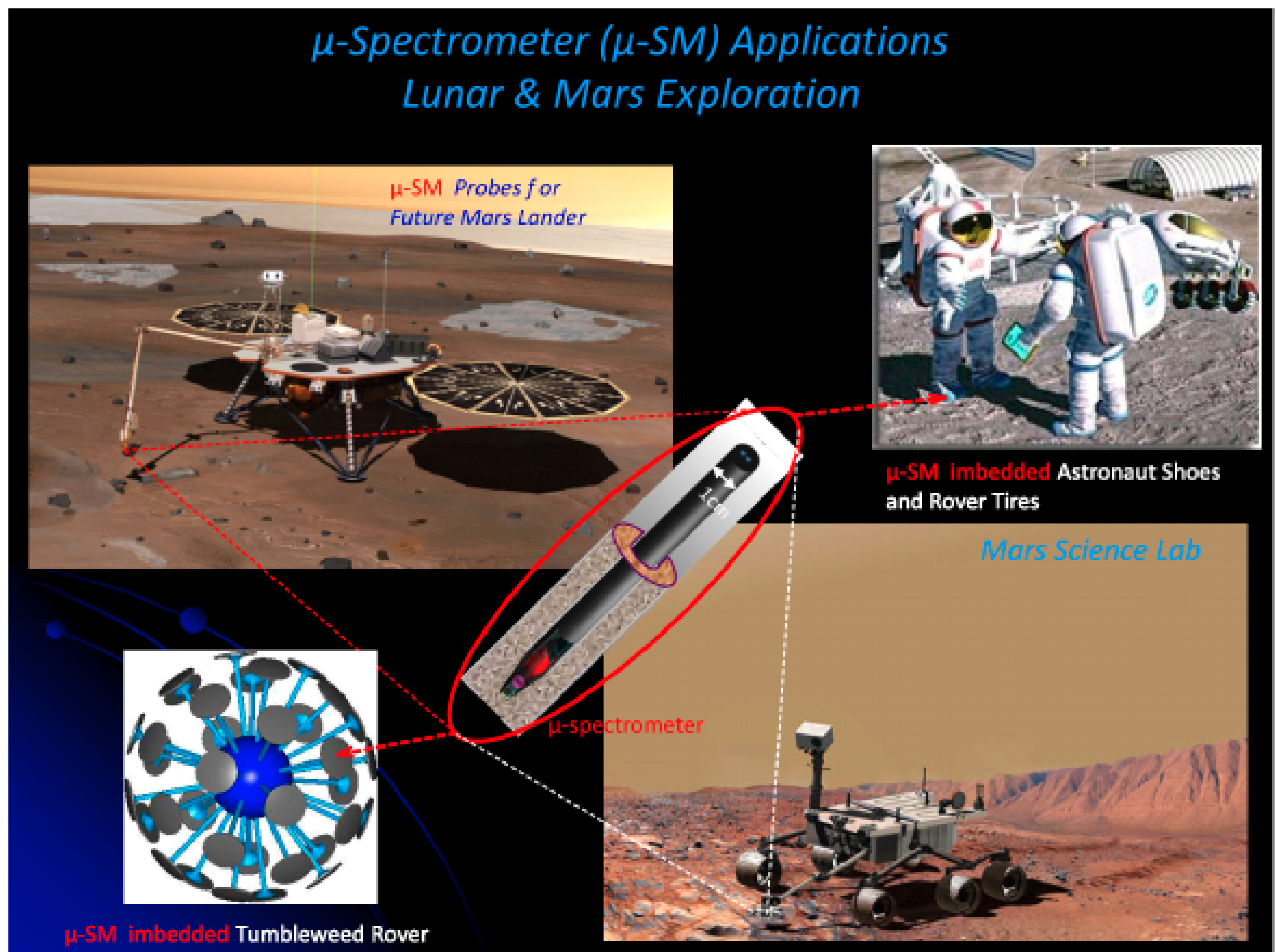

Fig. (2). In space exploration, micro-spectrometer (μ-SM) will be used to assay lunar and Martian soils as an autonomous satellite probe (upper left corner), a spike probe pegged into astronauts' shoes (upper right corner), a spike probe pegged into rover's tires like metal pegs of snow tires (lower right corner), or a tumble-weed sensor (lower left corner).

growth of the DBR layers in order to minimize the diffraction loss for lasing. For a sidewall edge emitting GaN laser diode, an RMS roughness of <17nm with a vertical alignment error of <2° is required to obtain 50% of the ideal Fresnel refractivity [14,15]. A GaN VCSEL structure with 100 DBR layers requires an even stricter RMS roughness per layer since the roughness is additive in the growth direction. The equivalent RMS roughness required per layer can be estimated to be $17\text{nm} / \sqrt{100\ layers} = 17\text{Å}$.

2. PROCESS AND CHARACTERIZATION

A dual column FIB system (FEI Company, Hillsboro, Oregon) was used to modify a rough GaN surface into a flat smooth surface in the nanometer scale. While other groups [16,17] have used a Ga^+ FIB as a vertical cutting tool to fabricate a sharp-edge vertical mirror, we used a Ga^+ FIB to make a horizontally flat surface by milling the surface material from perpendicular direction to the surface.

Multiple samples of GaN were grown on sapphire $Al_2O_3(0001)$ substrates by nitrogen plasma assisted molecular beam epitaxy (MBE) with a low-energy constricted-plasma source [18,19]. Using the nitrogen-rich operating conditions outlined in [19], we obtained the very rough GaN surfaces shown in Fig. (**3a**). It was reported that MBE grown GaN yields smooth surface morphologies under Ga rich conditions and rough surface morphologies under nitrogen rich conditions as a result of extensive columnar growth [20]. Growth under a Gallium rich condition is suitable for n-type materials grown with Si n-type dopant. The growth under a nitrogen rich condition is suitable for p-type materials grown with a magnesium dopant. An array of Ga^+ FIB processed areas were fabricated using a beam energy of 30 KeV. The angle of incidence was held constant at 90° and the beam current and the total etching time were varied as shown in Fig. (**3b**).

Another array of Ga^+ FIB processed areas were made with a low pressure iodine gas in order to enhance the etch rate [21]. The iodine gas was introduced into the processing area using a proximity nozzle so that the chamber was maintained at a pressure of 10^{-5} torr. The local pressure of iodine gas in the processing area was estimated to be a few milli-torr. Fig. (**4a**) shows a SEM image of the area processed using only the Ga^+ ion beam and Fig. (**4b**) shows

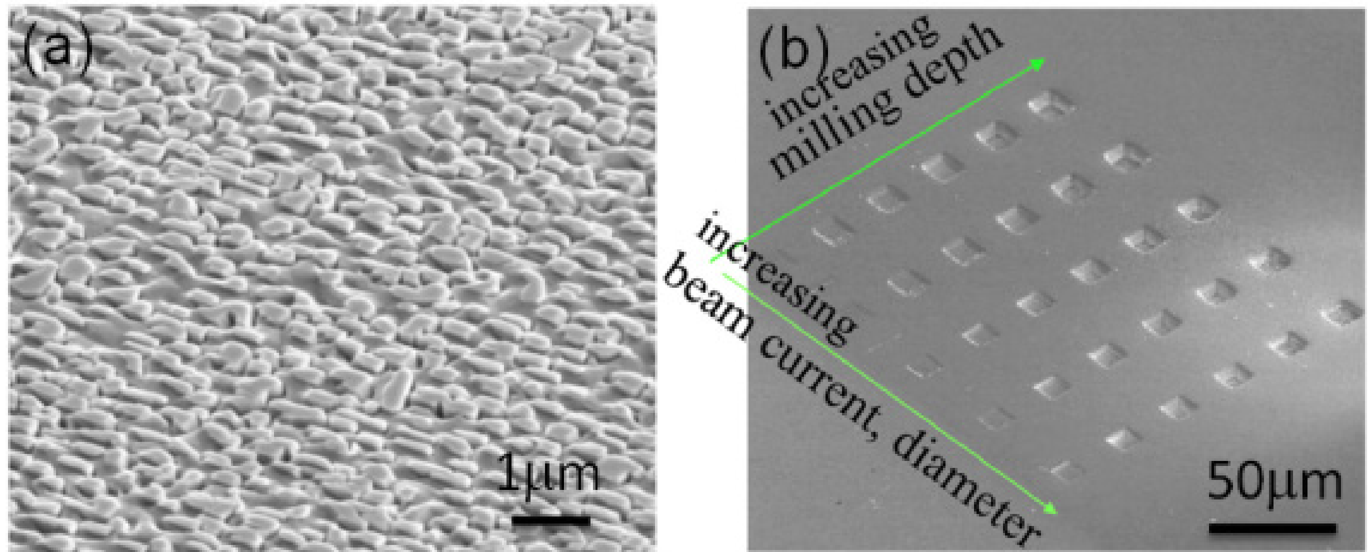

Fig. (3). (**a**) High resolution SEM image of a very rough GaN surface, which was grown by MBE under nitrogen rich conditions. (**b**) Low resolution SEM image of an array of processed areas by varying the ion beam current and the total etching time of the Ga^+ FIB.

another SEM image of the area processed using the Ga^+ ion beam in conjunction with the introduced iodine gas. The area processed with the Ga^+ ion beam alone shows the presence of residual materials and liquid Ga droplets. In contrast, the area processed with iodine gas and Ga^+ ion beam shows greatly improved flatness in the SEM image. The iodine gas helps to improve the flatness of the processed area by forming gaseous gallium iodide which assists in the removal of the liquid Ga droplet. When the GaN lattice is bombarded with a Ga^+ ion beam, nitrogen from GaN vaporizes and the remaining gallium liquefies on the surface resulting in the slightly rough surface in Fig. (**4a**). On the other hand, when iodine gas is supplied, the remaining liquid Ga reacts with the iodine gas to yield a volatile gas phase of gallium iodide, which leaves the substrate resulting in a surface with a lower surface roughness. While the boiling point of pure gallium is 2403°C, those of gallium iodides (GaI_3 and Ga_2I_6) are only 345°C. Thus, when the focal point of gallium ion beam impinges on the sample, the local temperature is increased to several hundred °C due to the kinetic energy of the 30KeV Ga+ ion beam in a narrow area. The gallium iodide thus becomes a vapor and leaves the surface. Therefore a smoother surface is obtained with the assistance of iodine gas. Chlorine gas can be another choice for etching gas to remove gallium droplet since gallium chloride has a very low boiling point of 201°C.

A simple calculation can be made for the steady-state local temperature rise assuming an adiabatic surface as shown in Fig. (**4c**). The generated heat (***q***) by bombardment of ion beam in spherical volume of radius (***r***) determines the local temperature (***T***) at the spherical surface. $\boldsymbol{T_s}$ is the substrate temperature at a radius ($\boldsymbol{r_s}$). Thermal conductivity of GaN is between 90 and 230 W/m·K depending on the doping concentration and dislocation density [22]. The thermal conductivity (***k***) of the sapphire substrate is 36 W/m·K [22]. Because the thickness of GaN is only a few micrometers and the sapphire substrate is very thick, ~ 500μm, the combined effective thermal conductivity can be set as ***k***=38 W/m·K. The steady-state thermal equation for spherical systems shows the local temperature (***T(r)***) is determined by the following thermal equation under an adiabatic surface condition [23],

$$T(r) = T_S + \frac{q}{4\pi k}\left[\frac{1}{r} - \frac{1}{r_S}\right] \tag{1}$$

Because the size of typical wafer is large compared with the thickness of GaN thin film, we can approximate the equation as $r_S \to \infty$,

$$T(r) = T_S + \frac{q}{4\pi k r} \tag{2}$$

Therefore, the local temperature (***T(r)***) is determined by the beam radius (***r***), the initial substrate temperature ($\boldsymbol{T_s}$), and the heat (***q***) generated by the ion beam. Assuming all of the ion beam's kinetic energy is converted into heat (***q***) which is confined in a radius (***r***), it is possible to calculate the local temperature (***T(r)***) as a function of the beam radius (***r***) as shown in the graph of in Fig. (**4d**). The graph of Fig. (**4d**) compares the vaporization point of gallium iodide to the calculated local temperature. ***T(r)*** rises more as the focal point is reduced. In this simple calculation, the local temperature becomes greater than the vaporization point of gallium iodide when the beam radius is smaller than 4nm. The actual temperature of the incoming Ga+ ions at the moment of collision is much hotter than the local temperature (***T(r)***) at the spherical surface due to the kinetic energy from the 30KeV ion beam.

Ion damage from the Ga^+ FIB into the bulk regions of the GaN is expected, but it can be repaired using a post-annealing process similar to post annealing processes performed after ion implantation. Furthermore, the embedded Ga^+ ion can be crystallized into GaN under a nitrogen plasma because it is not an extrinsic impurity in GaN.

Iodine has very high vapor pressure, 400 mtorr at room temperature and even higher pressure at elevated

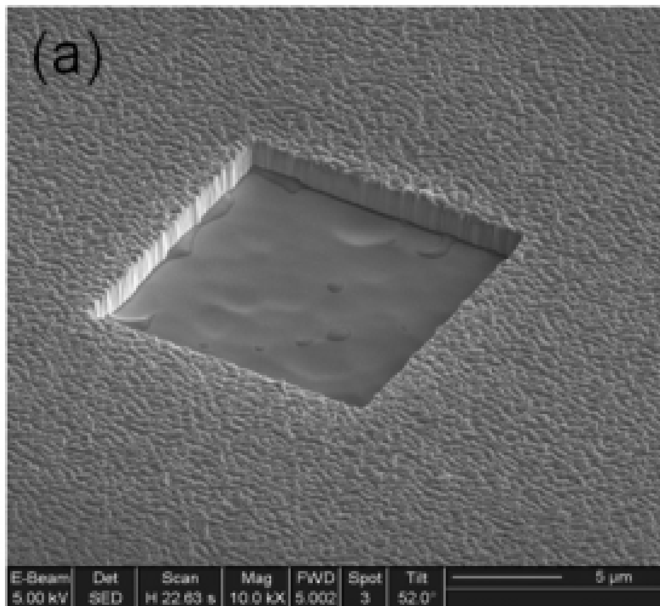

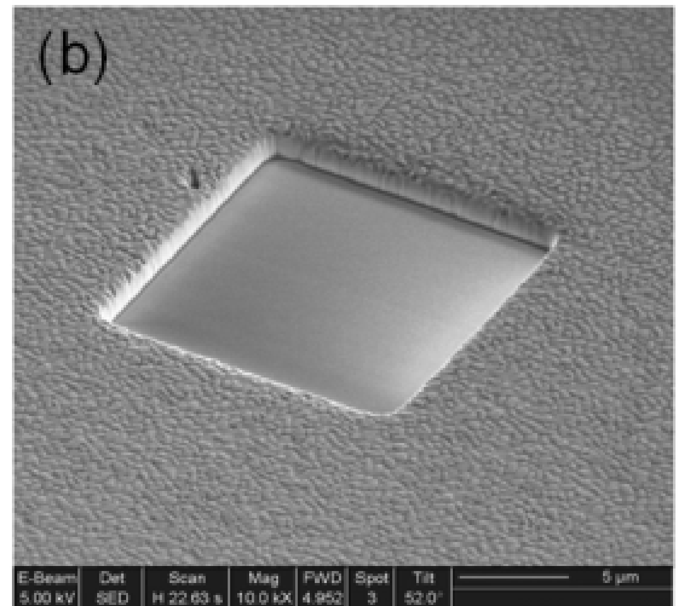

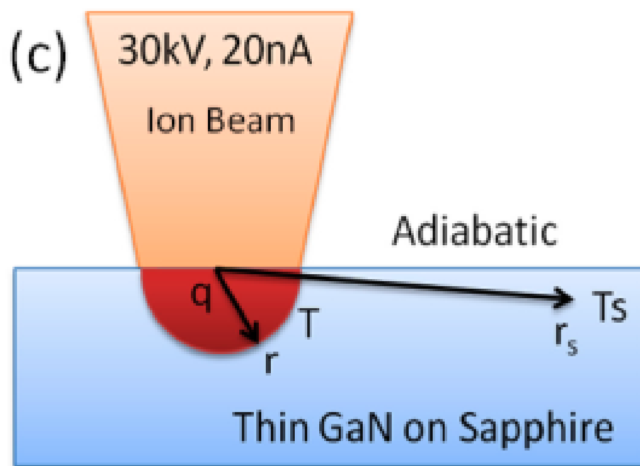

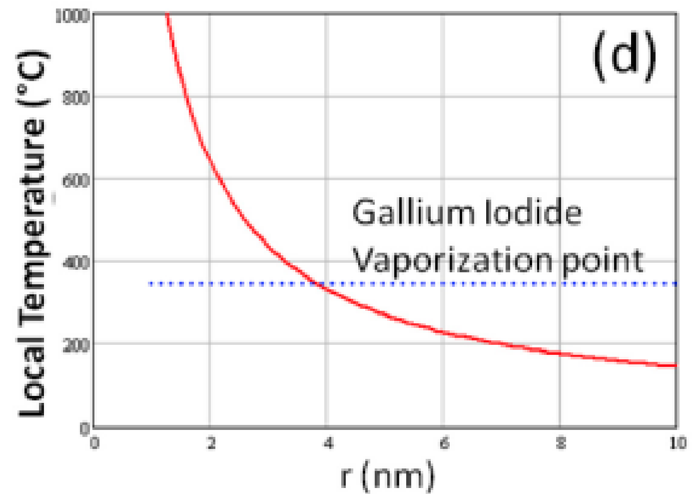

Fig. (4). SEM image of the GaN surface processed by (**a**) using only the Ga^+ ion beam (**b**) using the Ga^+ ion beam in conjunction with the introduced iodine gas, (**c**) thermal simulation model with a heat source in radius *r* at temperature *T* of thin GaN on a sapphire substrate, (**d**) maximum local temperature (*T*) rise *vs* radius of heat source made by ion beam.

temperatures so that it vaporizes fast on the surface without being incorporated into materials. A mild heating of substrate can remove iodine doping completely.

Since SEM measures only the secondary electron emission, and not the actual topography, AFM was used to characterize the actual surface topography of the Ga^+ ion beam processed areas. Fig. (**5a**) shows an AFM image of the area processed using a Ga^+ FIB with injected iodine gas. The parallel lines at the bottom surface are the etch ripples made by the scanning of the Ga^+ ion beam. Fig. (**5b**) shows a cross-sectional view of the AFM data. The broad hill at the bottom of the cross-sectional image indicates that the Ga^+ ion beam cannot completely eliminate nor flatten surface structures larger than the secondary ion diameter caused by the primary ion beam. On the other hand, the tiny structures seen in Fig. (**3a**) are completely eliminated and a very smooth surface was obtained.

The bombardment of energetic particles generates a volume of secondary ions and electrons described by Wright and Gruen [24,25]. The secondary ions and electrons enhance the diffusion process in the local surface region and form irregular ripples of residual materials. These irregular ripples formed by a broad ion beam are explained with surface diffusion process induced by kinetic energy of ion beams according to several theories including the MCB (Makeev, Cuerno, Barabasi) theory [26] and the BH (Bradley and Harper) theory [27]. Although irregular ripples made by a FIB have been described by Datta *et al*. [28], a

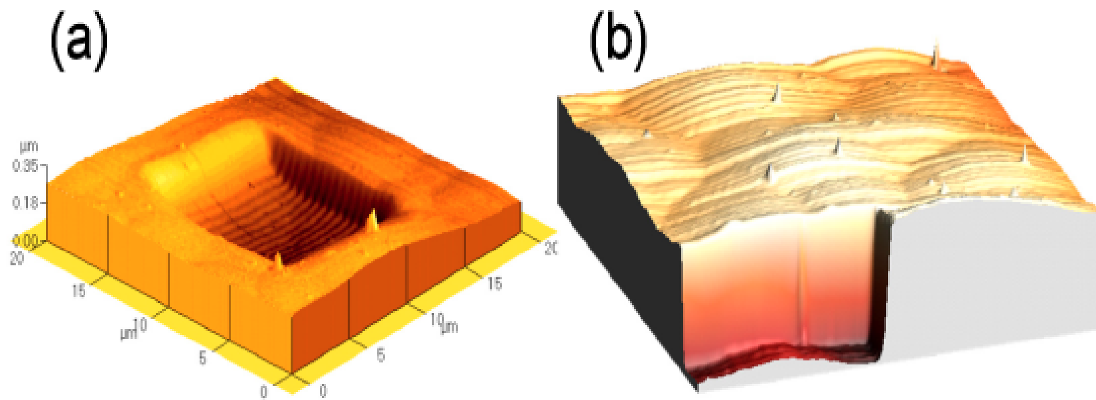

Fig. (5). (**a**) AFM image of a GaN surface processed using the Ga^+ FIB with iodine gas. Dark lines are geometric ripples along the slow-scan axis of FIB, (**b**) a cross-section view of the same surface (10µm × 10µm).

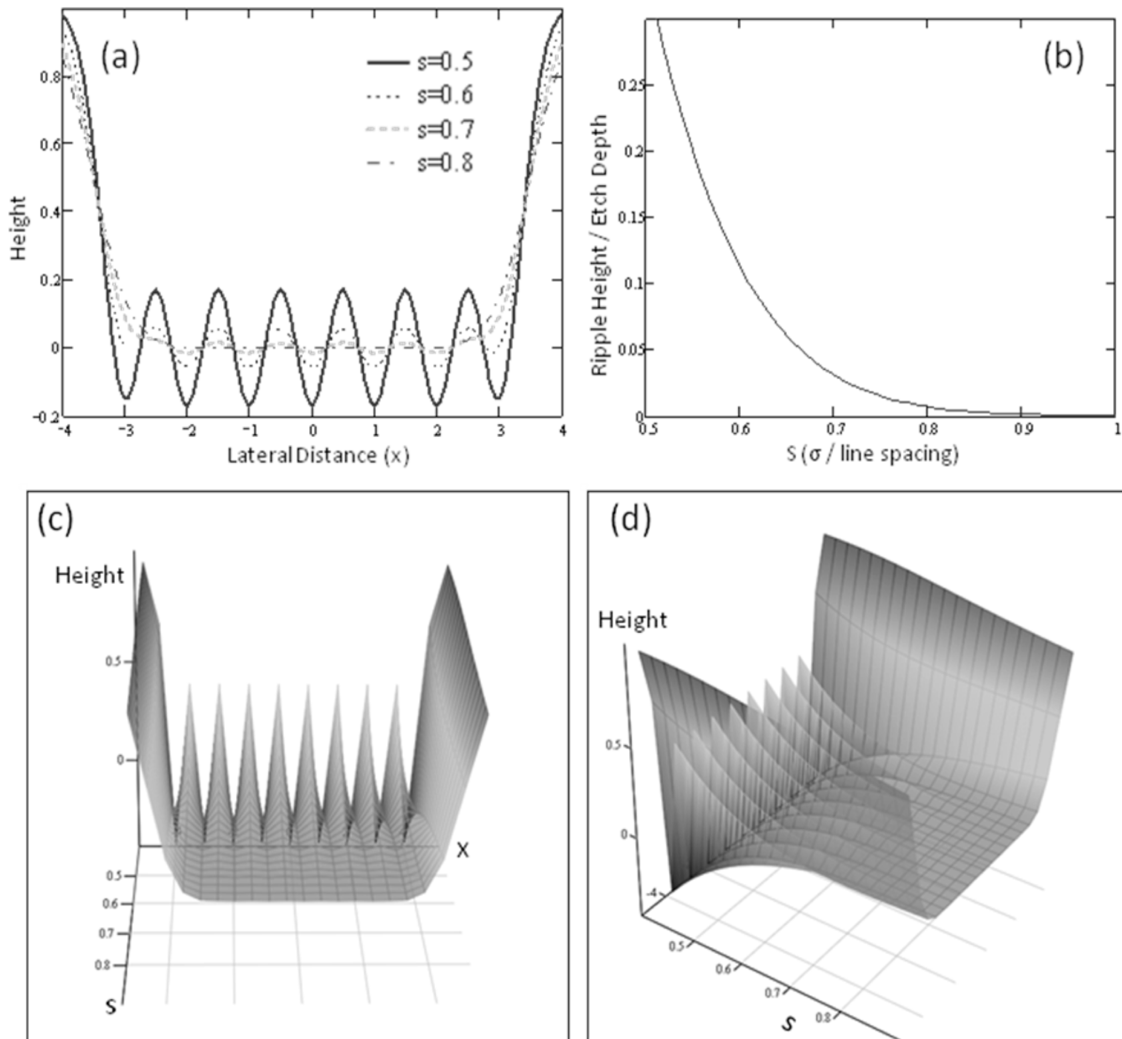

Fig. (6). (**a**) Simulated cutting profile with various ***s*** parameters, (**b**) normalized ripple height *vs* ***s*** parameter, (**c**) 3-D graph cutting profile with X-axis as the slow scan direction, Y-axis as various ***s*** parameters (***s***=0.4~0.9) and Z-axis as the height of remaining materials after cutting, (**d**) same 3-D graph in different viewing angle to show the dependence of ripple corrugation on ***s*** parameter (***s*=σ/*L***).

simple engineering model describing the regular geometric ripples formed by the overlapping of sequential FIB etching lines has not been fully developed. The ripples in our experiment are very regular and geometric, which are observed as the straight lines in Fig. (**5a**) and Fig. (**7a**), and the circular lines in Fig. (**1d**). Usually, the geometric ripples are aligned with the slow scan axis of the focused ion beam. An engineering model that is different from the MCB and BH theories is required to control the regular geometric ripple patterns.

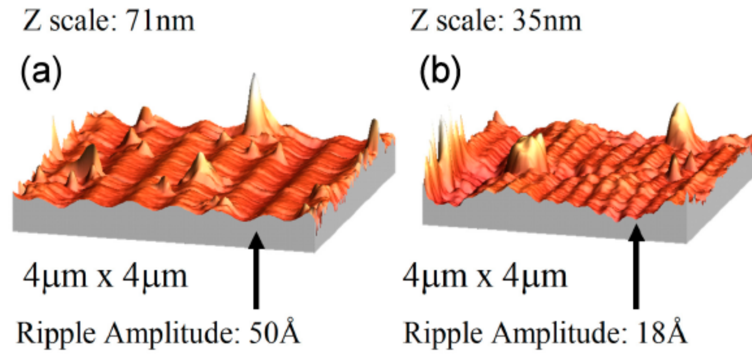

Fig. (7). AFM images of a GaN surface processed using the Ga^+ FIB with iodine gas, (**a**) beam voltage of 30KeV and beam current of 20nA, z-scale of 3D image: 71nm, (**b**) beam voltage of 30KeV and beam current of 7nA, z-scale of 3D image: 35nm.

It is likely that the geometric ripples along the slow scan axis are made by the superposition of multiple one-point Gaussian cutting profiles running along the fast scan axis. Therefore, a normalized cutting profile **g(s, x)** is approximated as a Gaussian normal distribution for a straight line cutting case:

$$g(s,x) = \frac{\exp\left[-(\frac{x}{s})^2\right]}{s \cdot \sqrt{\pi}} \quad (3)$$

where the parameter (***s***) is a ratio of the standard deviation (***σ***) over the cutting line spacing (***L***) on the slow scan axis, such that ***s*** = ***σ/L,*** and the variable (***x***) is the ratio of the lateral distance (***X***) over the line spacing (***L***) on the slow scan axis, such that ***x*** = X/***L***.

The normalized cutting depth, ***Depth(s, x, n)*** as a function of ***s, x,*** and the number of ripples (***2n+1***) is then described as,

$$Depth(s,x,n) = 1 - \sum_{m=-n}^{n} g(s, x+m)$$

The shape of the surface profile after cutting is shown in Fig. (**6a**) with different ***s*** parameters. When the standard deviation (***σ***) is small, ***s*** becomes small and the cutting depth profile becomes strongly rippled. As the standard deviation (***σ***) increases and approaches the width of the line spacing (***L***), the ***s*** parameter approaches 1, causing the corrugation to disappear. Fig. (**6b**) shows the dependence of the normalized ripple height on the ***s*** parameter. When ***s***=0.6, the ripple height is about 10% of cutting depth. When ***s***=0.7, the ripple height is less than 4% of the cutting depth.

Fig. (**6c**, **d**) show 3D graphs of the cutting profile. The normalized lateral distance (***X/L***) is on the X-axis and the ***s*** parameter (***σ/L***) is on the Y-axis. These graphs show how the corrugation ripple is related to the standard deviation of the one-point cutting profile.

The results presented here suggest that the ratio of the standard deviation (***σ)*** to the line spacing (***L***) determines the formation of ripple structures and the effective etching profile of the nano-milling processes. Therefore the ripple corrugation can be minimized by reducing the slow-scan axis line spacing (***L***) or increasing the standard deviation (***σ***).

In order to characterize the geometric ripples caused by the focused ion beam, high resolution 4μm × 4μm AFM images were taken at the bottom of the processed square and are shown in Fig. (**7**). In Fig. (**7a**), the ion beam current of 20nA was used with a 50% beam diameter overlap defined in the control software and etch-scanning rate of 8.85μm^3/s. In Fig. (**7b**), the ion beam current of 7nA was used with a 50% beam diameter overlap defined in the software and etch-scanning rate of 3.08μm^3/s. The measured surface corrugation ripple amplitudes were 50Å for the 20nA sample and 18Å for the 7nA sample. While the corrugation ripples in Fig. (**7a**) are straight lines, the observed ripples in Fig. (**7b**) are slightly irregular. Therefore, when the beam current is very low and line spacing is small, the ripples made by sequential focused ion beam milling show a transition from a geometrically aligned Gaussian profile model to the diffusion enhanced irregular ripple models described by BH and MCB theories [26-28].

3. CONCLUSION

We demonstrated the use of a Ga^+ FIB to mill epitaxially grown GaN layers at the nanoscale in order to prepare the surface for use as a DBR mirror growth structure. Tiny rough surface structures smaller than the ion beam cutting line spacing were eliminated and smoother surfaces were obtained with iodine gas injection. The smoother surface morphology obtained with the iodine gas injection was explained by the thermal evaporation of volatile gallium iodide compounds that form at the focal point. The GaN surfaces had their geometric ripple amplitude reduced from 50Å to 18Å after FIB processing with smaller beam current and line spacing. An engineering model to explain the regular geometric ripples was described using the sequential superposition of a one-point Gaussian cutting profile along the slow-scan axis. Additionally, topographic ripples made by focused ion beam scanning were characterized with AFM. Reducing the beam current and slow-scan axis line-spacing of the incident FIB reduces the corrugation ripple-amplitude and forms a smooth surface. Our study shows that the FIB nano-milling processed samples with a small line spacing (***L***) and large beam profile standard deviation (***σ***) can satisfy the surface flatness and roughness requirements for an AlGaN/GaN DBR structure.

ACKNOWLEDGEMENTS

This research was partly supported by the NASA space act agreement (SAA #15546), U.S.A. and the KOSEF program of Ministry of Education, Science, and Technology (MEST), the Republic of Korea. The authors acknowledge

support of the National Center for Electron Microscopy, Lawrence Berkeley Lab, which is supported by the U.S. Department of Energy under Contract # DE-AC02-05CH11231. The authors appreciate scientific discussion and help from Prof. Eicke Weber, Prof. Andrew Minor, and Dr. Velimir Radmilovic at U.C. Berkeley and National Center for Electron Microscopy, Lawrence Berkeley Lab.

REFERENCES

[1] Park Y, Choi SH, King GC, Elliott JR. Micro spectrometer for parallel light. NASA Case No. LAR 17425-1, August 28, 2006.

[2] Daniel JH, Moore DF, Walker JF. Focused ion beams and silicon-on-insulator - a novel approach to MEMS. Smart Mater Struct 2000; 9: 284-290.

[3] Park Y, Koch L, Song KD, Park SJ, King GC, Choi SH. Miniaturization of a Fresnel spectrometer. J Opt A Pure Appl Opt 2008; 10: 1-8.

[4] Nakamura S, Harada Y, Seno M. Novel Metalorganic chemical vapor-deposition system for GaN Growth. Appl Phys Lett 1991; 58: 2021-2023.

[5] Nakamura S, Fasol G. The Blue Laser Diode: GaN Based Light Emitters and Lasers. Springer: Berlin 1997.

[6] Nakamura S, Senoh M, Mukai T. High-power InGaN/GaN double-heterostructure violet light-emitting-diodes. Appl Phys Lett 1993; 62: 2390-2392.

[7] Someya T, Werner R, Forchel A, Catalano M, Cingolani R, Arakawa Y. Room temperature lasing at blue wavelengths in gallium nitride microcavities. Science 1999; 285: 1905-1906.

[8] Zhou HL, Diagne M, Makarona E. Near ultraviolet optically pumped vertical cavity laser. Electron Lett 2000; 36: 1777-1779.

[9] Kao CC, Peng YC, Yao HH, *et al.* Fabrication and performance of blue GaN-based vertical-cavity surface emitting laser employing AlN/GaN and Ta_2O_5/SiO_2 distributed Bragg reflector. Appl Phys Lett 2005; 87: 81-105.

[10] Nurmikko A, Han J. Blue and near-ultraviolet vertical-cavity surface-emitting lasers. MRS Bull 2002; 27: 502-506.

[11] He Y, Ozden I, Diagne M, *et al.* Blue and violet vertical cavity light emitters and multielement arrays. Compd Semicond 2002; 170: 157-164.

[12] Nosker RW, Mark P, Levine JD. Polar surfaces of wurtzite and zinc blende lattices. Surf Sci 1970; 19: 291.

[13] Mackowiak P, Sarzala RP, Wasiak M, Nakwaski W. An attempt to design room-temperature-operated nitride diode VCSELs. Opto-Electron Rev 2004; 12: 411-416.

[14] Ito T, Ishikawa H, Egawa T, Jimbo T, Umeno M. Fabrication of flat end mirror etched by focused ion beam for GaN-based blue-green laser diode. Jpn J Appl Phys 1997; 36: 7710-7711.

[15] Satome K, Honda T, Matsutani A, Koyama F, Iga K. Int. Sym. Blue Laser and Light Emitting Diodes, Chiba Univ. Japan, 1996; p. 506.

[16] Mack MP, Via GD, Abare AC, *et al.* Improvement of GaN-based laser diode facets by FIB polishing. Electron Lett 1998; 34: 1315-1316.

[17] Ambe C, Takeuchi T, Katoh H, *et al.* GaN-based laser diode with focused ion beam-etched mirrors. Mater Sci Eng B-Solid 1999; 59: 382-385.

[18] Anders A, MacGill RA, Brown IG, Vizir AA. Filamentless ion source for materials processing. Rev Sci Instrum 1998; 69: 880-882.

[19] Anders A, Kuhn M. Characterization of a low-energy constricted-plasma source. Rev Sci Instrum 1998; 69: 1340-1343.

[20] Kim Y, Subramanya SG, Siegle H. GaN thin films by growth on Ga-rich GaN buffer layers. J Appl Phys 2000; 88: 6032-6036.

[21] Chyr I, Steckl AJ. GaN focused ion beam micromachining with gas-assisted etching. J Vac Sci Technol B 2001; 19: 2547-2550.

[22] Mion C, Muth JF, Preble EA, Hanser D. Thermal conductivity: dislocation density and GaN device design. Superlattice Microstruct 2006: 40: 338-342.

[23] Incropera FP, DeWitt DP. Heat and Mass Transfer, New York: John Wiley & Sons 2002.

[24] Wright RB, Gruen DM. Discussion of the origin of secondary photon and secondary ion emission during energetic particle irradiation of solids.1. collision cascade. J Chem Phys 1980; 72: 147-171.

[25] Wright RB, Gruen DM. Secondary photon-emission studies of ion bombarded beryllium. Nucl Instrum Methods 1980; 170: 577-583.

[26] Makeev MA, Cuerno R, Barabasi AL. Morphology of ion-sputtered surfaces. Nucl Instrum Methods B 2002; 197: 185-227.

[27] Bradley RM, Harper JME. Theory of ripple topography induced by ion-bombardment. J Vac Sci Technol A 1988; 6: 2390-2395.

[28] Datta A, Wu YR, Wang YL. Real-time observation of ripple structure formation on a diamond surface under focused ion-beam bombardment. Phys Rev B 2001; 63: art. no.-125407.

Received: December 16, 2009 Revised: January 19, 2010 Accepted: February 18, 2010

© Park *et al.*; Licensee *Bentham Open*.

This is an open access article licensed under the terms of the Creative Commons Attribution Non-Commercial License (http://creativecommons.org/licenses/by-nc/3.0/) which permits unrestricted, non-commercial use, distribution and reproduction in any medium, provided the work is properly cited.